# Dispersion of the long-wavelength phonons in Ge, Si, GaAs, quartz, and sapphire

H.-Y. Hao and H. J. Maris
*Department of Physics, Brown University, Providence, Rhode Island 02912*
(Received 14 November 2000; published 10 May 2001)

We have used the picosecond ultrasonic technique to measure the dispersion of long-wavelength longitudinal acoustic phonons in Ge, Si, GaAs, z-cut quartz, and sapphire. In these experiments, a subpicosecond light pulse was used to generate a strain pulse at one surface of the sample. After propagation through the sample, the shape of this strain pulse was modified because of the phonon dispersion. From this change in shape, the magnitude of the dispersion could be determined. The results are compared with various lattice dynamical models. We also report on measurements of the temperature dependence of the sound velocity and the acoustic attenuation.

DOI: 10.1103/PhysRevB.63.224301 PACS number(s): 63.20.−e

## I. INTRODUCTION

Picosecond ultrasonics is a technique that uses short light pulses to generate and detect acoustic pulses.[1] Because of the excellent time resolution, it is possible to perform ultrasonic experiments on thin-film structures to which conventional ultrasonic pulse-echo methods cannot be applied. The frequency spectrum of the acoustic pulses that can be studied with this technique extends up to several hundred gigahertz. In a recent paper,[2] we have presented a variation of the picosecond ultrasonic technique that can be used to measure the dispersion of longitudinal acoustic phonons at long wavelengths. Results for Si and Ge were reported. In this paper we describe the experimental method in more detail, report results for several other crystals, and compare the data that we have obtained to different lattice dynamical models of these crystals.

## II. EXPERIMENT

The basic idea of the experiment is as follows. A short strain pulse is generated optically, and the shape of this pulse is measured after it has propagated through the crystal. For a traveling acoustic pulse, the components with higher frequencies will usually propagate at speeds slower than the sound velocity, and after a sufficient period of time this leads to the formation of an oscillating tail of the pulse. From the change in the shape of the pulse, the phonon dispersion can be determined.

The propagation of pulse disturbances in a crystal lattice was first considered by Baden-Powell[3] and by Hamilton.[4] Hamilton considered the problem of a linear chain of particles interacting via linear springs between nearest neighbors. At time $t=0$, all atoms were at rest at their equilibrium positions except for the atom at the origin that was given a displacement $A_0$. He showed that at a later time the displacement $u_n(t)$ of the $n$th atom was

$$u_n(t)=A_0 J_{2n}(\Omega_{\max}t), \tag{1}$$

where $J_{2n}$ is the Bessel function, $\Omega_{\max}=(4\beta/M)^{1/2}$ is the maximum phonon frequency, and $\beta$ is the strength of the springs. For a linear chain with interactions that extend beyond nearest neighbors, it is straightforward to show that the displacement is given by the more general formula

$$u_n(t)=\frac{A_0 a}{\pi}\int_0^{\pi/a}\cos(qan)\cos(\omega_q t)\,dq, \tag{2}$$

where $\omega_q$ is the frequency of a phonon with wave number $q$, and $a$ is the lattice parameter. For nearest neighbor forces, $\omega_q=\Omega_{\max}\sin(qa/2)$, and the result of Eq. (1) is recovered from Eq. (2).

It is interesting to evaluate the result of Eq. (2) for large times, i.e., for $\omega_q t\gg 1$. The distance traveled by the pulse will then be much greater than the lattice parameter. Also the pulse will have spread out to have a width much larger than $a$. It is then more convenient to work in terms of the distance $x$ along the chain, and to treat this as a continuous variable. Thus, we need to consider the displacement $u(x,t)$, which we can write in the form

$$u(x,t)=\frac{A_0 a}{2\pi}\int_0^{\pi/a}[\cos(qx-\omega_q t)+\cos(qx+\omega_q t)]\,dq. \tag{3}$$

We first consider $x>0$. For large $t$, the main contribution to the integral will come from values of $q$ such that the argument of one of the cosines is nearly stationary. Thus, the second cosine term can be neglected. For the first term, the argument will be stationary when $x=v_q t$, where $v_q\equiv\partial\omega_q/\partial q$ is the group velocity. Thus, if the dispersion is normal, i.e., if $v_q$ decreases monotonically as $q$ increases, there will be no value of $q$ for which the argument is stationary unless $t\geqslant t_0$, where $t_0\equiv x/c$ is the arrival time for low-frequency components, and $c$ is the sound velocity. Hence, for $t\leqslant t_0$ the value of the integral will be small. For values of $t$ only slightly greater than $t_0$, the value of $q$ at which the argument of the first cosine is stationary will be much less than $\pi/a$. We can expand the dispersion relation in the form

$$\omega_q=cq-\gamma q^3+\cdots, \tag{4}$$

where $\gamma$ is a coefficient that describes the dispersion to lowest order. The value of $q$ that corresponds to the stationary argument is $q_s$, which is then given by

 

$$q_s = \sqrt{\frac{c}{3\gamma t}(t-t_0)} \cong \sqrt{\frac{c}{3\gamma t_0}(t-t_0)}. \tag{5}$$

Given that the most important contribution to the integral comes from the region around $q_s$, we then find

$$u(x,t) \approx \frac{A_0 a}{2(3\gamma t_0)^{1/3}} \mathrm{Ai}\left[ -c\frac{t-t_0}{(3\gamma t_0)^{1/3}} \right], \tag{6}$$

where Ai is the Airy function. The Airy function decreases rapidly when its argument becomes positive, i.e., for $t<t_0$. For a negative argument the Airy function is an oscillatory function. For $t>t_0$, we can express the Airy function in terms of a modulus $M$ and a phase $\theta$, giving[5]

$$u(x,t) = \frac{A_0 a}{2(3\gamma t_0)^{1/3}} M\left[ -c\frac{t-t_0}{(3\gamma t_0)^{1/3}} \right] \times \cos\left[ \theta\left( -c\frac{t-t_0}{(3\gamma t_0)^{1/3}} \right) \right]. \tag{7}$$

For large values of its argument, the phase $\theta$ has the asymptotic expansion[5]

$$\theta(y) \approx \frac{3\pi}{4} - \frac{2y^{3/2}}{3} + \frac{5}{48y^{3/2}} \cdots. \tag{8}$$

Hence, from Eqs. (7) and (8), we see that the frequency $\Omega$ of the oscillations in $u_n(t)$ when $t>t_0$, and $t-t_0 \ll t_0$ is

$$\Omega(t) = \left| \frac{d\theta}{dt} \right| = \sqrt{\frac{c^3(t-t_0)}{3\,\gamma\, t_0}} = \sqrt{\frac{c^4(t-t_0)}{3\,\gamma\, x}}. \tag{9}$$

In order for Eq. (9) to hold, the conditions $t_0 \gg t-t_0 \gg \Omega^{-1}$ must be satisfied. We see that a measurement of the frequency of the oscillations can be used to give the dispersion parameter. The above analysis concerns the shape of a disturbance that initially involves just one atom. Consider now an ultrasonic experiment in which a pulse of width $\Delta x$ is generated. The form of such a pulse after it has propagated will be the convolution of the initial pulse shape with the pulse shape calculated in Eq. (6). Clearly, if the starting width of the ultrasonic pulse is too great, the oscillations in the tail of the pulse due to dispersion will be washed out. We can estimate how narrow a pulse is needed in order for dispersion effects to be visible. Consider, for example, a pulse of starting width $\Delta x$. This will contain wave numbers up to approximately $q_{\max} = (\Delta x)^{-1}$. After such a pulse has traveled a total distance of $x$, the highest frequency components will have fallen behind the lowest-frequency components by a distance that is of the order of $x\gamma q_{\max}^2/c$. For the effects of dispersion on the pulse shape to be visible, it is necessary that $x\gamma q_{\max}^2/c > \Delta x$. Therefore, it is necessary for the propagation distance to exceed

$$x_{\min} = \frac{c(\Delta x)^3}{\gamma}. \tag{10}$$

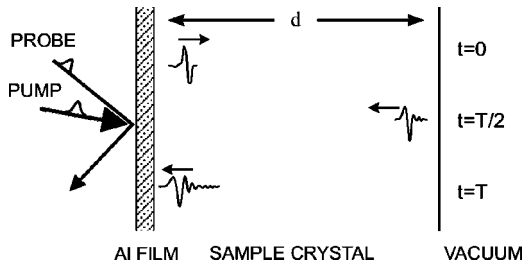


FIG. 1. Schematic diagram of the experiment. A light pulse is absorbed in the Al film and an acoustic pulse is generated. The pulse propagates across the crystal and is reflected at the far surface. The pulse returns to the Al transducer with a shape modified by dispersion, and is detected by a probe light pulse.

This same condition can also be arrived at by considering the convolution mentioned above. The order of magnitude of $\gamma$ is typically $10^{-11}$ $\mathrm{cm^3\,s^{-1}}$. From Eq. (10), it can be seen that for a pulse of width 1 mm, the propagation distance has to be of the order of $10^{14}$ cm in order for dispersion to be important. To see dispersion effects over a path length in the range of a few millimeters, it is necessary for $\Delta x$ to be of the order of 100 Å.

### A. Experimental technique

A schematic diagram of the experiment is shown in Fig. 1. The sample is a wafer of the crystal to be studied with both faces highly polished. An Al film is deposited onto one side of the wafer and is used as a transducer. An optical pump pulse of duration 200 fs is focused onto an area of about 25 $\mu$m in diameter on the Al film, and abruptly raises the local temperature by a few kelvins. This sets up a thermal stress, and this stress launches a longitudinal acoustic pulse into the sample. The acoustic pulse travels across the crystal, and is reflected with a sign change at the far surface. When the pulse reenters the Al transducer film, it causes a small change $\Delta R$ in the optical reflectivity of the film. By using a time-delayed optical probe pulse to measure $\Delta R(t)$ as a function of time $t$, we can measure the shape of the acoustic echo.

A Ti:sapphire mode-locked laser is employed as the optical source. The wavelength is 800 nm, and the time between pulses of 13.25 ns. Since the change of reflectivity is very small $(\Delta R(t)/R \sim 10^{-5})$, lock-in techniques are used to improve signal to noise. The travel time for the first acoustic pulse is very long (usually above 100 ns), and it would be inconvenient to produce a probe pulse with this delay through the use of a conventional optical path. Instead, as a probe pulse we have used a later pulse from the laser that has been given a further delay by means of a short adjustable optical path. For example, to achieve a delay of 100 ns, we use the seventh pulse (delayed by 92.75 ns) with an optical path delay of 7.25 ns.

In the experiment, the ultrasonic pulse has to travel for a few millimeters to show the effect of dispersion. At room temperature, the attenuation of sound in the frequency range of interest here (50–200 GHz) is very large. This attenuation is due to anharmonic interactions with thermal phonons. It is

TABLE I. A summary of the results obtained for the dispersion. $d$ and $c$ are the sample thickness and sound velocity, respectively. $\gamma_{exp}$ and $\gamma_{theory}$ are the experimental and theoretical values of the dispersion parameter defined in Eq. (4). The experimental results for $\gamma$ are compared with the values obtained from the theoretical models indicated by the superscripts.

| Sample | $d$ (cm) | $c$ ($10^5$ cm s$^{-1}$) | $\gamma_{exp}$ ($10^{-11}$ cm$^3$ s$^{-1}$) | $\gamma_{theory}$ ($10^{-11}$ cm$^3$ s$^{-1}$) | | |
|---|---|---|---|---|---|---|
| Si [100] | 0.200 | 8.48 | $1.80\pm0.05$ | 0.65 [a] | 1.07 [b] | 2.20 [c] |
| Si [110] | 0.504 | 9.18 | $8.45\pm0.15$ | 1.61 [a] | 6.55 [b] | 8.00 [c] |
| Si [111] | 0.210 | 9.40 | $2.60\pm0.08$ | 1.09 [a] | 3.42 [b] | 3.52 [c] |
| Ge [100] | 0.099 | 4.97 | $0.85\pm0.04$ | 0.41 [a] | 0.85 [b] | 1.50 [c] |
| Ge [110] | 0.099 | 5.46 | $5.55\pm0.08$ | 1.01 [a] | 4.63 [b] | 5.52 [c] |
| Ge [111] | 0.104 | 5.62 | $1.05\pm0.05$ | 0.68 [a] | 2.13 [b] | 2.46 [c] |
| GaAs [100] | 0.496 | 4.77 | $0.74\pm0.03$ | 1.05 [d] | | 1.34 [c] |
| GaAs [110] | 0.495 | 5.28 | $8.15\pm0.40$ | 2.25 [d] | | 4.44 [c] |
| GaAs [111] | 0.496 | 5.44 | $1.20\pm0.05$ | 1.16 [d] | | 2.28 [c] |
| $SiO_2$ [0001] | 0.201 | 6.40 | $7.75\pm0.05$ | 6 [e] | | |
| $Al_2O_3$ [0001] | 0.107 | 11.23 | $3.50\pm0.30$ | 2.0 [f] | | |

[a]Nearest-neighbor model of Hsieh (Ref. 15).
[b]Born-von Karman model with 31 parameters by Tamura (Ref. 16).
[c]Adiabatic-bond-charge model by Weber (Ref. 17).
[d]Rigid-ion model by Tamura and Harada (Ref. 18).
[e]Extended-shell models (Ref. 20).
[f]Shell model by Schober *et al.* (Ref. 21).

therefore necessary to perform the experiment below about 70 K to diminish the attenuation problem.[6]

When the energy per pulse is below a critical value $E_c$, a small variation in the energy changes the amplitude of the echo, but does not change the echo shape. Above $E_c$, the echo shape begins to change as the energy is increased. We believe this is due to nonlinear elastic effects arising from the finite amplitude of the elastic strain.[7] The critical energy $E_c$ varied from one sample to another. Since the nonlinear elastic effects increase with increasing propagation distance, it is to be expected that the critical energy will be less in thicker samples. The critical energy will also be lower in materials with larger third-order elastic constants. The effect of a variation in the energy of the pump light pulses was investigated and will be reported in detail in a separate paper.

### B. Samples

Measurements were made for Ge, Si, and GaAs with [100], [110], and [111] orientations, z-cut quartz, and sapphire (see Table I). All the samples were highly polished to reduce diffuse scattering of the sound pulse. Surface roughness is expected to scatter the higher-frequency components in the pulse strongly. To investigate this, we took data on two different pieces of 2-mm-thick [100] Si, sample (a) with a good surface polish and sample (b) with a much rougher surface. The data are shown in the inset to Fig. 2. For the rough surface sample, no oscillations are visible in the tail of the pulse. Figure 2 also shows the absolute magnitude $\Delta R(\nu)$ of the Fourier transform of the first returning echo for these two samples. It can be seen that for sample (b) the high frequency components are much weaker than for sample (a).

For each sample, an Al thin film of thickness 240–300 Å was deposited onto one side as an ultrasonic transducer. Films in this thickness range generate acoustic pulses with peak frequency around 120 GHz. The Al films were deposited by using a magnetron sputter gun in a cryopumped system achieving a base pressure of $10^{-8}$ torr. In this type of experiment, it is very important that the transducer film be well bonded to the sample. The quality of the adhesion between the Al film and the sample can be determined by measuring $\Delta R(t)$ in the first 30 ps after the application of the pump light pulse. If the Al is poorly bonded, it will ''ring.''[8]

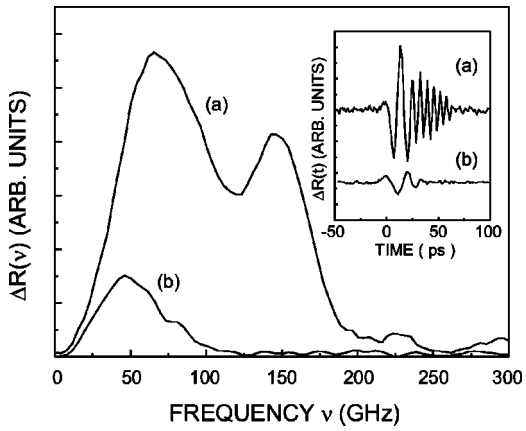


FIG. 2. Measurements on samples with (a) good, and (b) poor surface polish. The inset shows measurements of the reflectivity change as a function of time for the first acoustic echo. Time is measured from the front of the echo. The main part of the figure shows the magnitude $\Delta R(\nu)$ of the Fourier transform of the echo for the two samples.

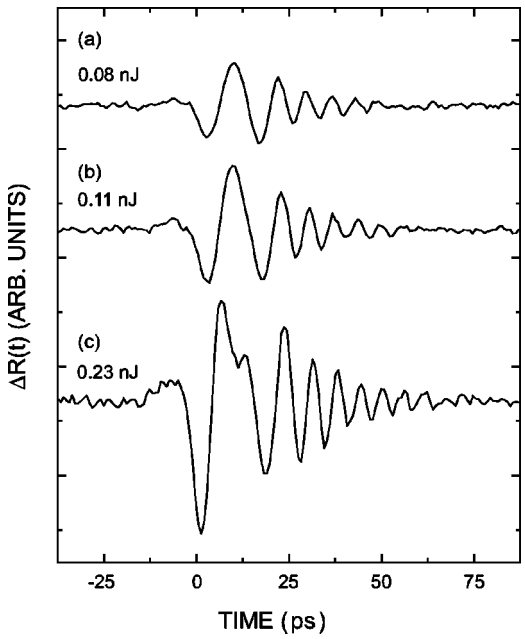


FIG. 3. Measurements of the change in reflectivity $\Delta R(t)$ for the first acoustic echo in a 2.1-mm Si [111] crystal at 25 K. The time scale has been offset so that zero corresponds to 443 900 ps. The energy of the pump light pulses for each data set is indicated.

### C. Data analysis

As an example of experimental data, we show in Fig. 3 a measurement of the first echo in a 2.1-mm-thick [111] Si sample. These data were taken at 25 K. In 3(a) we have used a pump pulse with energy incident onto the sample of 0.08 nJ. For a pulse energy of 0.11 nJ, the amplitude has increased but the pulse shape remains almost the same [see 3(b)]. In 3(c), the pulse energy is 0.23 nJ, and there is now a substantial distortion of the entire front of the pulse, while the period of the oscillations in the tail still remains the same. It is likely that nonlinear phenomena have a bigger effect on the front of the pulse simply because the amplitude is largest there. All measurements of the dispersion were made under conditions such that the period of the oscillations in the tail was unaffected by the pulse energy.

To determine the dispersion parameter from the data, a computer simulation of the shape of the echo was performed. The first step of the simulations was the calculation of the shape of the acoustic pulse generated by the Al film. This was done along the same lines as in Refs. 1 and 8, with the modification mentioned below. The temperature rise $\Delta\Theta(z)$ in the Al film induced by the pump light pulse as a function of the distance $z$ into the film was determined. This depends on the absorption length $\zeta$ of the pump light, and also on the rate at which hot electrons diffuse in Al.[9–11] For films of thickness in the range studied here, the temperature rise $\Delta\Theta(z)$ is approximately constant throughout the film thickness. From the temperature rise, the known elastic constants and thermal expansion coefficient, the stress in the Al film can then be found. The shape of the strain pulse that enters into the substrate can then be calculated in a straightforward way from elasticity theory. The acoustic pulse shape $\eta_{zz}^{(0)}(z)$ calculated in this way contains step discontinuities at some values of $z$. These discontinuities arise because it has been implicitly assumed that the stress in the Al film jumps discontinuously from zero to a finite value immediately after the pump light pulse has been absorbed. In reality, there will be a certain finite time interval $\tau_{\text{stress}}$ over which the stress will increase; $\tau_{\text{stress}}$ will be determined by the duration of the pump light pulse and by the time it takes the excited electrons to lose their energy to the thermal phonons in the Al film.[9–11] The duration of the pump light pulse was 0.2 ps and the time for energy transfer from the electrons is roughly the same. In 0.2 ps sound travels a distance of only 12 Å in Al, and so the effect of the finite value of $\tau_{\text{stress}}$ is unimportant.

The second step is the determination of the shape that the strain pulse has after it has propagated through the sample. To do this, we find the Fourier transform $\eta_{zz}(q,t=0)$ of the strain pulse when this pulse first enters the sample at time zero. At a later time $t$, the Fourier component becomes

$$\eta_{zz}(q,t)=\eta_{zz}(q,t=0)\exp(-i\omega_q t-\alpha_q t), \tag{11}$$

where $\omega_q$ is the dispersion relation in Eq. (4), and $\alpha_q$ is the rate at which the Fourier component $q$ attenuates with time. Then by performing the inverse Fourier transform, we obtain the pulse shape $\eta_{zz}(z,t)$ for time $t$. The change in the optical reflectivity $\Delta R(t)$ that takes place when the acoustic pulse reenters the Al film can be written as[12]

$$\Delta R(t)=\int f(z)\,\eta_{zz}(z,t)dz, \tag{12}$$

where $f(z)$ is called the sensitivity function, which can be calculated in terms of the optical constants (i.e., the dielectric constant and piezo-optic coefficients) of the Al film.[12] In the experiment, the measured quantity is the convolution of $\Delta R(t)$ with the time profile of the probe light pulse, but this convolution results in a negligible change in the shape of the $\Delta R(t)$.

The adjustable parameters are the dispersion $\gamma$, the thickness $d_{\text{Al}}$ of the Al film, the thickness $d$ of the sample (see details below), the attenuation $\alpha_q$, the optical constants of the Al film, and the intensity of the pump and probe beams on the surface of the sample. The intensity of the pump and probe beams on the surface of the sample affects only the magnitude of $\Delta R(t)$, not the variation of $\Delta R(t)$ with $t$. Of the other adjustable parameters, for all of the sample crystals except sapphire, only $\gamma$ has a significant effect on the frequency of the oscillations after the arrival of the main echo. Adjustment of the other parameters is important in order to obtain a good fit to the shape of the front of the pulse. Inclusion of the attenuation is necessary in order to reproduce the rate at which the oscillations in the tail of the echo damp out. For sapphire, the choice of the thickness of the Al film does affect the frequency of the oscillations in the tail of the pulse and the best-fit value for $\gamma$ (see discussion below).

In Figs. 4–7, we show measurements of $\Delta R(t)$ for the first echo in crystals of Si, Ge, $SiO_2$, and $Al_2O_3$, along with the computer simulations using parameters that give the best fit. The temperature at which these data were taken ranged from 25 to 35 K (see figure captions). In each figure, the time is measured relative to the $t_0$ indicated in the figure. In these

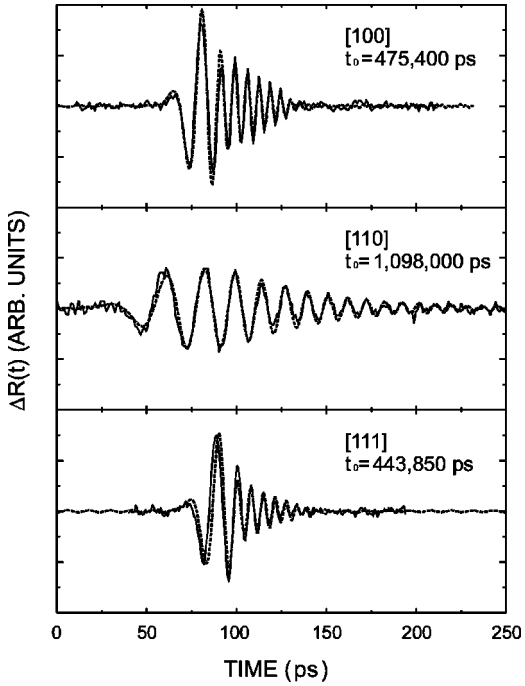


FIG. 4. Dispersion of longitudinal acoustic pulses in Si. The solid lines are the picosecond ultrasonic data and the broken lines are simulation results. Data are taken along three symmetry axes at 25 K. The time is measured relative to the time $t_0$ indicated for each trace.

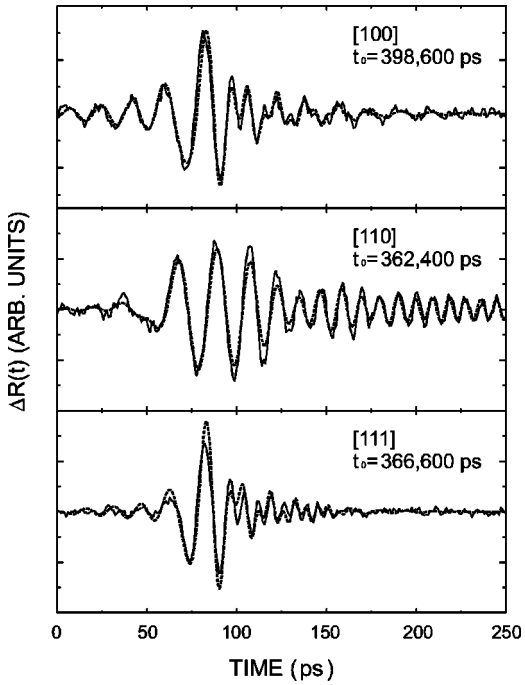


FIG. 5. Dispersion of longitudinal acoustic pulses in Ge along three symmetry axes at 25 K. The solid lines are the picosecond ultrasonic data and the broken lines are the simulations. The time is measured relative to the time $t_0$ indicated for each trace.

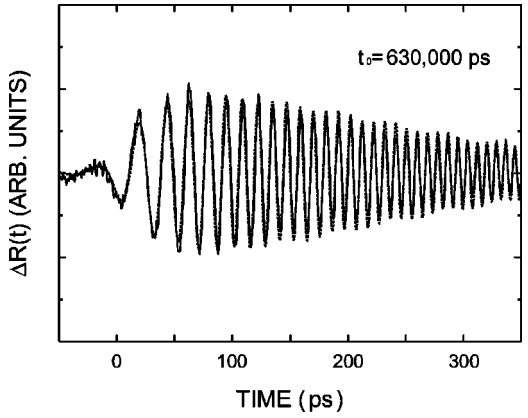


FIG. 6. Dispersion of longitudinal acoustic pulses in quartz along *z* axis at 25 K. The solid line is the picosecond ultrasonic data and the broken line is simulation result. The time is measured relative to the time $t_0$ as indicated.

computer simulations the attenuation was taken to vary as $q^2$. Note that this attenuation may arise from damping of the sound in the bulk of the sample or from the roughness of the sample surface.

Figure 4 shows the data for Si. Note that for the [110] sample, the frequency of the oscillations in the tail of pulse is much lower than that for the [100] and [111] directions. This is partly because the [110] sample is more than twice as thick as the other samples, but it is also a reflection of the larger value of $\gamma$ for the [110] direction. Data for Ge are shown in Fig. 5. For Ge, the analysis of the data is made more difficult by the presence of an extra contribution to the signal that has a constant frequency. This oscillation is readily apparent in the time range before the arrival of the main pulse for the [100] and [111] samples (see Fig. 5). For the [110] sample, it cannot be clearly identified in the plot of $\Delta R(t)$, but it shows up as a peak in the Fourier transform $\Delta R(\omega)$. This extra contribution arises from the component of the probe light pulse that passes through the Al transducer, is reflected at the

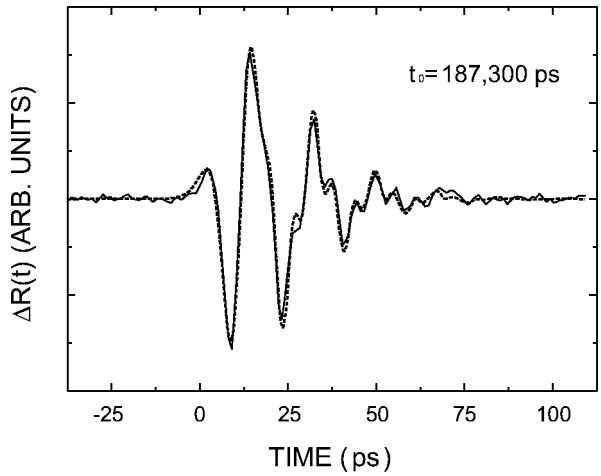


FIG. 7. Dispersion of longitudinal acoustic pulses in sapphire along *z* axis at 35 K. The solid line is the picosecond ultrasonic data and the broken line is simulation result. The time is measured relative to the time $t_0$ as indicated.

propagating strain pulse in the Ge, and then returns through the Al film. This component interferes with the component of the probe pulse that is reflected at the Al film. The two components of the probe pulse interfere destructively or constructively according to the distance $z$ that the strain pulse is below the surface. Hence, the intensity of the reflected probe light undergoes a periodic oscillation as the strain pulse propagates. It is straightforward to show that the frequency of the oscillation is $2nc\cos(\theta)/\lambda_0$, where $n$ and $c$ are the refractive index and sound velocity in Ge, respectively, $\lambda_0$ is the probe wavelength in free space, and $\theta$ is the propagation direction of the probe light in the Ge.[12] For a wavelength of 800 nm, $n$ is 4.5.[13] In the [100] direction, for example, the sound velocity is $4.97\times10^5$ cm s$^{-1}$, and the calculated frequency is 56 GHz, in good agreement with the measured frequency of 57 GHz in this direction. The amplitude of the oscillation is determined by the amplitude of the part of the probe light that is reflected at the propagating strain pulse. This amplitude is determined by (1) the attenuation suffered by the probe light as it passes twice through the Al film, (2) by the optical absorption of the probe light as it travels through the Ge to and from the instantaneous location of the strain pulse, and (3) by the piezo-optic coefficients of the Ge. The differences in the amplitude of the oscillations that are seen in the three crystallographic directions may reflect the anisotropy of the piezo-optic coefficients,[14] or instead may simply be a result of small differences in the thickness of the Al films on the three samples. Because of the presence of this component in the signal, in order to analyze the Ge data, it was necessary to perform a more elaborate simulation that allowed for the light penetration into the Ge. It can be seen from Fig. 5 that this gives a good fit to the data over the entire time range. It was necessary to apply a similar analysis for GaAs, but not for any of the other samples.

Data for z-cut quartz and sapphire are shown in Figs. 6 and 7. Quartz has an acoustic impedance that is close to the impedance of the Al transducer, and the stress that is set up in the Al by the pump light pulse propagates across the interface into the $SiO_2$ without significant reflection. As a consequence, the shape of the strain pulse that enters into the quartz is very simple, and the echo shown in Fig. 6 contains oscillations in the tail of the pulse that decrease smoothly in amplitude and have a steadily increasing frequency, as expected from Eq. (9). For $Al_2O_3$, on the other hand, the acoustic impedance is about 2.5 times the impedance of Al. Hence, the generated stress bounces back and forth in the Al before being transmitted into the sample. This gives rise to the complicated shape of the sound echo in $Al_2O_3$. To make a good fit to the echo shape, it is necessary to adjust the thickness of the Al transducer.

For the sound velocity, we have used literature values measured by conventional ultrasonic techniques. These values are typically accurate to $\pm0.1\%$. The nominal thickness $d$ of each sample was measured to an accuracy of $\pm5$ $\mu$m at room temperature by calipers, and is listed in Table I. However, in the experiment the arrival time of the first echo is measured with an accuracy of better than part in $10^5$. Hence, in making the fit to the data, it was necessary to adjust the value of $d$ to a much more precise value within the $\pm5$-$\mu$m range. For most of the samples, measurements of the dispersion were made over the temperature range from 25 to 70 K. Although we have observed a time shift of the echo due to the change of the sound velocity with temperature, no evidence for a change in the value of the dispersion parameter was found.

## III. RESULTS

### A. Dispersion results

The values of the dispersion parameter $\gamma_{\rm exp}$ that give the best fit are listed in Table I. The uncertainty in these values depends mostly on the signal-to-noise ratio.

For comparison, we have also listed in Table I for each crystal the dispersion parameter $\gamma_{\rm theory}$ that is obtained from different lattice dynamical models.[15–21] Each of these models contains a number of parameters that in the original papers were chosen so that the model gave a good fit to the phonon dispersion curves as measured by inelastic neutron scattering. For Si, Ge, and GaAs, we recalculated the dispersion relations and confirmed the results that had been obtained in the original papers. We then calculated $\omega_q$ for very small $q$, and obtained $\gamma_{\rm theory}$ by fitting $\omega_q$ to the form given in Eq. (4). For quartz and sapphire, the lattice dynamical models are complex, and we did not repeat the calculation of the dispersion relation. Instead, we obtained $\gamma_{\rm theory}$ simply by making a fit of Eq. (4) to the small $q$ part of the dispersion curves as given in the figures of Refs. 19 and 21.

Hsieh[15] constructed two models for Si and Ge, one with nearest-neighbor forces only, and the other adding in a central force interaction between next-nearest neighbors. Table I includes the values of $\gamma$ calculated for Hsieh's nearest neighbor model. It can be seen that the measured dispersion is larger than the theoretical value by a factor that varies from 1.5 for Ge [111] to 5.5 for Ge [110]. This discrepancy is not unexpected since $\gamma$ is very sensitive to the long-range part of the interatomic forces.[22] To see this, consider the linear chain with springs of strength $\beta_n$ connecting an atom to its $n$th nearest neighbors. For this system the dispersion relation is given by

$$\omega_q^2=\frac{4}{M}\sum_{n=1}^{\infty}\beta_n\sin^2\left(\frac{nqa}{2}\right). \tag{13}$$

The sound velocity $c$ and the dispersion parameter $\gamma$ are then

$$c=\left(\frac{1}{M}\sum_{n=1}^{\infty}\beta_n n^2a^2\right)^{1/2}, \tag{14}$$

$$\gamma=\frac{1}{24Mc}\sum_{n=1}^{\infty}\beta_n n^4a^4. \tag{15}$$

Because of the factor of $n^4$ in Eq. (15), long-range forces make a greater contribution to $\gamma$ than they do to $c$. A number of models have been constructed to include long-range forces in an approximate way. For Si and Ge, Tamura[16] has constructed a model of the Born–von Karman type with interactions extending out to eighth-nearest neighbors. This in-

troduces 31 parameters that are then adjusted so that a good fit to the dispersion curves as measured by neutron scattering is obtained. These models give much larger values of $\gamma$, in the same general range as is found experimentally (see Table I). The difference between experiment and theory is largest for Si [100] ($\gamma_{\rm exp}/\gamma_{\rm theory}=1.68$) and Ge [111] ($\gamma_{\rm exp}/\gamma_{\rm theory}=0.49$). The other model that we have investigated in detail is the adiabatic bond-charge model of Weber.[17] This model is in fairly good agreement with the experimental data for Si (average deviation of 17%), but overestimates the value of $\gamma$ for Ge [100] and [111] by about a factor of 2.

For GaAs, the measured $\gamma$ shows a very strong anisotropy, such that the ratio of $\gamma_{110}$ to $\gamma_{100}$ is 11. We have compared the data with the adiabatic bond-charge model of Weber[17] and a rigid ion model of Tamura and Harada.[18] These models give only a fair agreement with the data (see Table I). It can be seen that although the models predict correctly that the dispersion is largest in the [110] direction and smallest in [100], they substantially underestimate the anisotropy of $\gamma$.

For quartz, we compare the experimental $\gamma$ with the value extracted from a shell-model calculation performed by Schober *et al.*[20] The shell model [model SM(4)] gives a very good fit for the neutron-scattering data over most of the phonon spectrum, but has difficulty in reproducing the correct sound velocities. Schober *et al.*[20] have suggested that this discrepancy might come about because ultrasonic techniques measure the velocity of first sound, whereas neutron scattering are made in the zero-sound regime. To estimate the dispersion, we have made a fit of Eq. (4) to the theoretical result for the longitudinal acoustic branch as plotted in Fig. 2 of Ref. 19. The fit was made over the range of wave vectors extending out to one quarter of the distance to the zone boundary. The result that is obtained is in reasonable agreement with experiment (see Table I).

The result for sapphire has been compared with $\gamma$ found for the shell model by Schober *et al.*[21] The theoretical value of $\gamma$ was found by making a fit to the published dispersion curve (Fig. 3 of Ref. 21), using the form of Eq. (4) and again fitting the published curve over the range from $q=0$ out to one quarter of the distance to the boundary of the Brillouin zone. As already discussed, the experimental value for sapphire has a much bigger uncertainty than for the other samples. The accuracy could be substantially improved if a thicker sample were used.

### B. Temperature dependence of the sound velocity

By measuring how the arrival time of the echo varies with temperature, we can make an accurate determination of the temperature-dependence of the sound velocity $c$. The variation of $c$ with temperature was found to be largest for the materials with low Debye temperature (Ge, GaAs, and $SiO_2$), and least for sapphire ($\Theta_D=1030$ K). This variation is to be expected because of the higher density of thermal phonons in the materials with low $\Theta_D$. Data for all of the samples are shown in Fig. 8. The sound velocity change shown here is not corrected for the thermal expansion of the sample. These measurements were made from the lowest temperature at which data could be taken up to the temperature at which the ultrasonic attenuation became so large that acoustic echoes could no longer be detected.

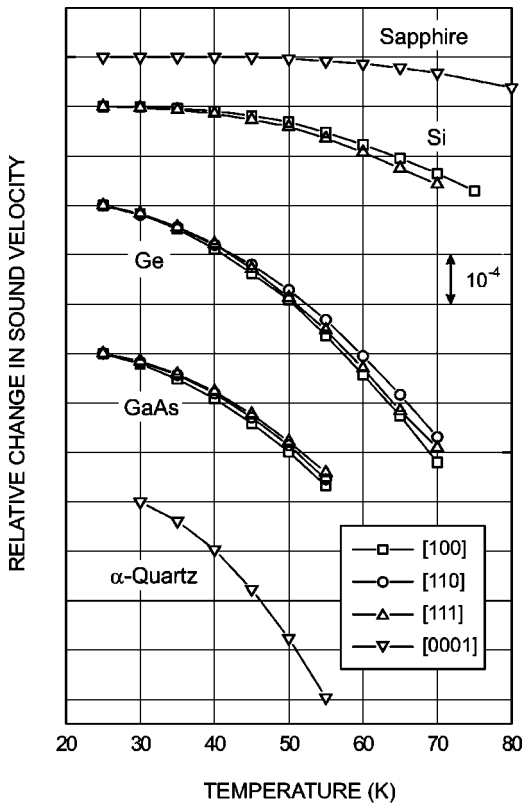


FIG. 8. Relative change in the longitudinal sound velocity $\Delta c(T)/c(T=0)$ in $Al_2O_3$, Si, Ge, GaAs, and $SiO_2$ with temperature. The data for the different samples have been offset for clarity. The scale for the sound velocity change is as indicated on the figure.

The change of the sound velocity with temperature can be divided into two components. The first component arises from the thermal expansion. Whenever a crystal is strained, there is a change in the sound velocity that can be calculated using a well-known formula involving the strain and the second- and third-order elastic constants.[23] The thermal expansion of the crystal amounts to a temperature-dependent strain of the sample, and thus causes a change in sound velocity. This first component is independent of the frequency of the sound wave. The second component arises from anharmonic interactions between the sound wave and the thermal phonons. This component depends on the sound frequency and takes different forms according to the value of $\omega\tau$, where $\omega$ is the sound frequency and $\tau$ is the thermal phonon relaxation time.[24,25] In the measurements reported here, the frequency is so high that $\omega\tau$ is much greater than unity over the entire temperature range in which measurements were made. However, conventional ultrasonic measurements at 1 MHz, for example, are in the $\omega\tau\ll 1$ regime.[24,25] Thus, the temperature dependence measured in this experiment should differ from that measured by low-frequency ultrasonics. Let us define the difference in velocity as $\Delta c(T)\equiv c(T)-c(T=0)$. It is expected theoretically that $\Delta c(T)$ for $\omega\tau\gg 1$ will be positive with respect to $\Delta c(T)$ for $\omega\tau\ll 1$.[24,25]

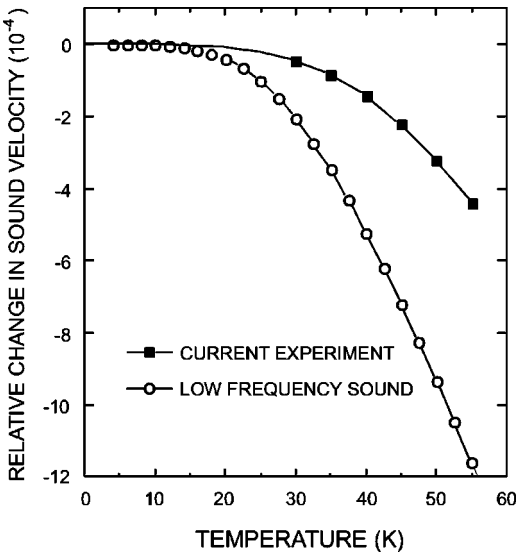


FIG. 9. Temperature-dependent part of the sound velocity change in quartz as measured in the megahertz frequency range (open squares) from Ref. 26, and measured at high frequency in the present experiment (solid squares).

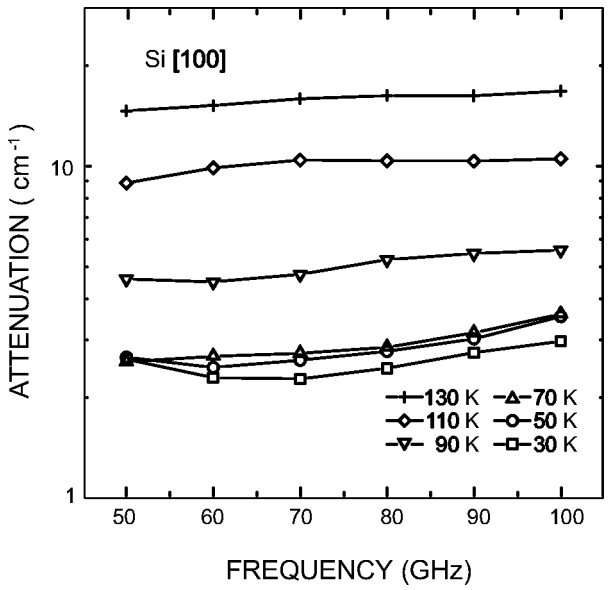


FIG. 10. Attenuation of longitudinal acoustic phonons in the [100] direction of Si.

The only material for which we have been able to find accurate low-frequency data with which to make a comparison is z-cut $SiO_2$. Measurements were made at 5 and 10 MHz by Smagin and Mil'shtein[26] using a resonant oscillator method. They obtain data down to 4 K, and their results are shown in Fig. 9. To compare the temperature-dependence that they have measured with the results that we have obtained, we have extrapolated our data to $T=0$ K on the basis of a $T^4$ law[27] to estimate $\Delta c_{\omega\tau\gg1}(T)$. It can be seen from Fig. 9 that $\Delta c_{\omega\tau\gg1}(T)$ is always positive with respect to $\Delta c_{\omega\tau\ll1}(T)$, as expected theoretically.[25]

### C. Attenuation

In the fits to the data shown in Figs. 4–7, it has been assumed for simplicity that the attenuation of the Fourier component $q$ varies as $q^2$. By analyzing the Fourier spectrum of the acoustic echoes, we can obtain more detailed information about the attenuation of phonons in the GHz range. Let $\Delta R_1(t)$ and $\Delta R_2(t)$ be the changes in optical reflectivity due to the first and second acoustic echoes, and let $\Delta R_1(\omega)$ and $\Delta R_2(\omega)$ be the Fourier transforms of these echoes. The attenuation per unit distance of the Fourier component of frequency $\omega$ is then

$$\alpha(\omega)=\frac{1}{2d}\ln\left|\Delta R_1(\omega)/\Delta R_2(\omega)\right|. \tag{16}$$

The attenuation determined in this way includes attenuation within the sample, and also any losses that occur when the strain pulse is reflected at the surfaces. The wavelength of 100-GHz sound in Ge, for example, is approximately 500 Å, and so it is certainly reasonable to expect that there will be losses arising from the roughness of the sample surface.

As already noted, the attenuation increases rapidly with temperature, and the ultrasonic echoes disappear at high temperatures. Accordingly, to measure attenuation over as wide a temperature range as possible, it was advantageous to use thinner samples than were used for the dispersion measurements. Data taken on a Si [100] wafer of thickness 315 $\mu$m are shown in Fig. 10. Reliable measurements of $\alpha(\omega)$ are possible only for the frequencies such that both $\Delta R_1(\omega)$ and $\Delta R_2(\omega)$ can be accurately measured, and for this sample this fact restricted the frequency range from 50 to 100 GHz. The attenuation below 70 K is nearly independent of temperature, and we assume that this arises from either surface losses or defects in the sample. The temperature-dependent part of the attenuation is essentially independent of frequency, and increases rapidly with increasing temperature. Note also that at least in this sample, the attenuation at low temperatures (i.e., in the temperature range within which the dispersion measurements were made) does not vary as $\omega^2$ as assumed in the simulations.

As far as we are aware, there are no other measurements of the ultrasonic attenuation in Si in this frequency-temperature range. Pomerantz[28] has made measurements at 9.1 GHz up to 60 K, and Keller[29] has obtained data at 3.1 GHz up to 100 K, and at 0.64 GHz up to room temperature. At 100 K, the attenuation was found to increase by about a factor of 6 between 0.64 and 3.1 GHz. The attenuation at 3.1 GHz and 100 K is smaller than the attenuation that we have measured by about a factor of 5.[30]

The attenuation of sound due to anharmonic interactions with thermal phonons has been reviewed by Maris.[25] In the range of frequency and temperature involved here, the sound frequency $\omega$ is such that $\omega\tau\gg1$, where $\tau$ is the average lifetime of the thermal phonons. When this condition is satisfied, one approach is to consider the sound to be composed of low-energy phonons that undergo collisions with thermal phonons. In these collisions, energy and momentum must be

conserved. It can be shown that these conservation laws have the consequence that the only possible collisions are those in which a longitudinal sound phonon collides with a thermal phonon with transverse polarization and a transverse phonon of different polarization is produced.[31] This type of collision is called a Herring process. It is unlikely that the attenuation that we have measured is due to the Herring process. The attenuation by this mechanism is predicted to vary as $\omega^2$, whereas we find an attenuation independent of frequency. In addition, an estimate of the magnitude of the effect indicates that it is at least two orders of magnitude smaller than the measured attenuation.[32]

There is also a relaxation contribution to the attenuation that arises from the finite lifetime of the thermal phonons. For $\omega\tau \gg 1$, this contribution can be approximated by the result

$$\alpha(\omega) = \frac{CT}{2\rho c^3 \tau}[\langle \gamma_G^2 \rangle - \langle \gamma_G \rangle^2], \tag{17}$$

where $C$ is the specific heat, $\rho$ is the density, $\gamma_G$ is the Grüneisen constant, and the averages $\langle \cdots \rangle$ are over the thermal phonon spectrum.[25] This contribution to the attenuation is independent of frequency, as is found experimentally. The value of $\tau$ can be estimated from the thermal conductivity.[33] In Fig. 11, we show a fit of Eq. (17) to the experimental data at 90, 110, and 130 K. The data have been averaged over the frequency range 50–100 GHz. To obtain this fit it is necessary to assume a value of 12 for the quantity $\langle \gamma_G^2 \rangle - \langle \gamma_G \rangle^2$. This is larger than expected since calculations of Grüneisen constants for Si by Mayer and Wehner[34] give values that vary substantially over the phonon spectrum, but have magnitudes of unity or less for nearly all phonons. However, it is interesting to note that Keller[29] obtained a value of 19.8 for $\langle \gamma_G^2 \rangle - \langle \gamma_G \rangle^2$ from an analysis of his attenuation measurements at 0.64 GHz.

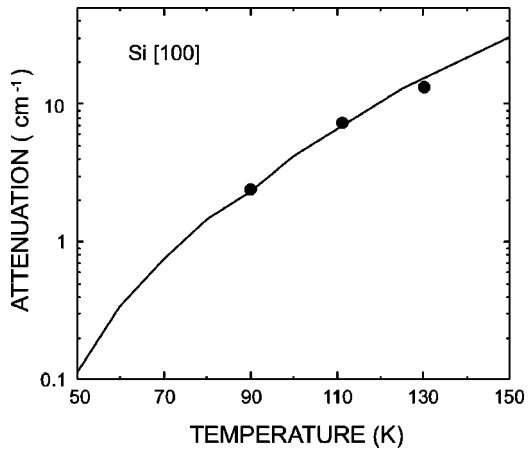


FIG. 11. Temperature-dependent part of the attenuation in the [100] direction of Si as a function of temperature. The solid circles are the experimental data and the solid curve is a fit based on Eq. (17) as described in the text.


## ACKNOWLEDGMENTS

We thank Professor S. Tamura for sending us his programs for calculating the dispersion for Si, Ge, and GaAs. We also thank Professor W. Weber for providing information about the adiabatic bond-charge model calculation for GaAs. This work was supported in part by the U. S. Department of Energy through Grant No. DE-FG03-ER45267.



[1] C. Thomsen, H.T. Grahn, H.J. Maris, and J. Tauc, Phys. Rev. B **34**, 4129 (1986).

[2] H.-Y. Hao and H.J. Maris, Phys. Rev. Lett. **84**, 5556 (2000).

[3] J. Baden-Powell, *View of the Undulatory Theory as Applied to the Dispersion of Light* (J. W. Parker, London, 1841).

[4] W.R. Hamilton, *Mathematical Papers* (Cambridge Univ. Press, London, 1940).

[5] *Handbook of Mathematical Functions*, edited by M. Abramowitz and I.A. Stegun (National Bureau of Standards, Washington, 1964).

[6] For example, at room temperature the attenuation length for 56 GHz longitudinal sound in GaAs is about 26 $\mu$m. See W. Chen, Z.R. Wasilewski, S. Tamura, and H.J. Maris, Philos. Mag. B **70**, 687 (1994).

[7] H.-Y. Hao and H.J. Maris, Physica B **263-264**, 670 (1999).

[8] G. Tas, J.J. Loomis, H.J. Maris, A.A. Bailes, and L.E. Seiberling, Appl. Phys. Lett. **72**, 2235 (1998).

[9] G. Tas and H.J. Maris, Phys. Rev. B **49**, 15 046 (1994).

[10] V.E. Gusev, Opt. Commun. **94**, 76 (1992).

[11] O.B. Wright and V.E. Gusev, IEEE Trans. Ultrason. Ferroelectr. Freq. Control **42**, 331 (1995); V.E. Gusev and O.B. Wright, Phys. Rev. B **57**, 2878 (1998).

[12] H.-N. Lin, R.J. Stoner, H.J. Maris, and J. Tauc, J. Appl. Phys. **69**, 3816 (1991).

[13] This is the refractive index of Ge at 800 nm and 120 K as measured by R.F. Potter, Phys. Rev. **150**, 562 (1966).

[14] G. Theodorou and G. Tsegas, Phys. Rev. B **56**, 9512 (1997).

[15] Y-C. Hsieh, J. Chem. Phys. **22**, 306 (1954).

[16] S. Tamura, Phys. Rev. B **28**, 897 (1983).

[17] W. Weber, Phys. Rev. B **15**, 4789 (1977); K.C. Rustagi and W. Weber, Solid State Commun. **18**, 673 (1976).

[18] S. Tamura and T. Harada, Phys. Rev. B **32**, 5245 (1985).

[19] D. Strauch and B. Dorner, J. Phys.: Condens. Matter **5**, 6149 (1993).

[20] H. Schober, D. Strauch, K. Nützel, and B. Dorner, J. Phys.: Condens. Matter **5**, 6155 (1993).

[21] H. Schober, D. Strauch, and B. Dorner, Z. Phys. B: Condens. Matter **92**, 273 (1993).

[22] M.P. Kemoklidze and L.P. Pitaevskii, Zh. Éksp. Teor. Fiz. **59**, 2187 (1970) [Sov. Phys. JETP **32**, 1183 (1971)].

[23] R.N. Thurston and K. Brugger, Phys. Rev. **133**, 1604 (1964).

[24] J.S. Blinick and H.J. Maris, Phys. Rev. B **2**, 2139 (1970).

[25] H.J. Maris, in *Physical Acoustics*, edited by W.P. Mason and R.N. Thurston (Academic, New York, 1971), Vol. VIII, p. 279.

[26] A.G. Smagin and B.G. Mil'shtein, Kristallografiya **19**, 832 (1975) [Sov. Phys. Crystallogr. **19**, 514 (1975)].
[27] It follows from Eqs. (111) and (226) of Ref. 25 that for $T \ll \Theta_D$, the leading term in the temperature dependence of the sound velocity should be proportional to $T^4$.
[28] M. Pomerantz, Phys. Rev. **139**, A501 (1965).
[29] K.R. Keller, J. Appl. Phys. **38**, 3777 (1967).
[30] Note that we are discussing here just the temperature-dependent part of the attenuation.
[31] C. Herring, Phys. Rev. **95**, 954 (1954). A variety of processes involving four or more phonons are also possible.
[32] This estimate was made along the same lines as in Ref. 6.
[33] R.J. Stoner and H.J. Maris, Phys. Rev. B **47**, 11 826 (1993).
[34] A.P. Mayer and R.K. Wehner, Phys. Status Solidi B **126**, 91 (1984).